Giant moisture responsiveness of a new conductive coordination polymer based chemiresistive sensor

Yuan Lin,[a,b] Huijie Jiang,[c] Guangling Liang,[a] Wei-Hua Deng[a,b], Qiaohong Li[*,a] Wen-Hua Li[*,a], Gang Xu[a]

[a]*State Key Laboratory of Structural Chemistry, Fujian Institute of Research on the Structure of Matter, Chinese Academy of Sciences (CAS). 155 Yangqiao Road West, Fuzhou, Fujian 350002, P. R. China*

[b]*University of Chinese Academy of Sciences, Chinese Academy of Sciences, Beijing 100049, China*

[c]*Institute of Materials in Electrical Engineering 1 (IWE1), RWTH Aachen University, Sommerfeldstrasse 24, 52074 Aachen, Germany.*

**Corresponding authors.*

E-mail: whli@fjirsm.ac.cn, lqh2382@fjirsm.ac.cn

Electronic conductivity measurement

The compound 1 single crystal device was fabricated using silver paste as the electrode, and two 50 μm diameter gold wires attached on the silver paste as the conducting wires.

The impedance measurements

To investigate the humidity sensitive mechanism of Ag(SPh-NO_2)•$AgNO_3$, AC impedance spectroscopy from 0.1 Hz to 10^5 Hz at various humidity was measured. The humidity and temperature are controlled by the constant temperature humidity chamber. The impedance measurements were measured by IMPEDANCE/GAIN-PHASE ANALYZER (SI 1260).

The DC instantaneous reverse polarity experiments

The corresponding DC circuit was shown in Figure S9 with the bias voltage of 5 V in Kethley 2602B source meter. The polarity of the bias was set instantaneous reversed between -5V and +5V with duration time of 60 seconds. The humidity sensor connected to DC will form the space charge acting as the conductive ions. When the polarity of DC was changed, the dominating conductive ions transferred to the opposite pole, leading to a current peak when they reached the other electrode.

Calculations of activation energy (*E_a*)

For semiconductors, the activation energy (Ea) is typically obtained by fitting temperature–dependent conductivity data to the Arrhenius equation :

$$\sigma = \sigma_0 \exp(-\frac{E_a}{kT})$$

where σ is conductivity, σ_0 is a prefactor, k is Boltzmann constant, T is temperature/K.[38]

Calculations of coefficient of variation

The coefficient of variation (CV) is defined as: CV = R_{SD} / $R_{average}$ ×100%, where R_{SD} and $R_{average}$ are the standard deviation (SD) and average value of responses with four successive cycles.

Table S1. Selected bond angels for compound **1**.

Bond	Length (Å)	Bond	Length (Å)
Ag(1)-S(1)#1	2.5823(15)	O(2)-N(1)	1.221(7)
Ag(1)-S(1)#2	2.5595(15)	O(1)-N(1)	1.221(7)
Ag(1)-S(1)#3	2.8147(16)	N(2)-O(3)	1.248(5)
Ag(1)-O(5)	2.519(4)	N(2)-O(4)	1.226(6)
Ag(2)-S(1)	2.5057(16)	N(1)-C(4)	1.474(6)
Ag(2)-O(3)	2.527(5)	C(1)-C(2)	1.384(6)
Ag(2)-O(3)#4	2.515(5)	C(1)-C(6)	1.388(7)
Ag(2)-O(5)#4	2.537(4)	C(6)-C(5)	1.382(7)
Ag(2)-O(2)#5	2.653(5)	C(2)-C(3)	1.381(7)
S(1)-Ag(1)#6	2.8146(16)	C(4)-C(3)	1.360(8)
S(1)-Ag(1)#1	2.5823(15)	C(4)-C(5)	1.362(8)
S(1)-Ag(1)#2	2.5595(14)	C(3)-H(3)	0.9300
S(1)-C(1)	1.765(4)	C(6)-H(6)	0.9300
O(5)-Ag(2)#7	2.537(4)	C(5)-H(5)	0.9300
O(3)-Ag(2)#7	2.515(5)	C(2)-H(2)	0.9300
O(5)-N(2)	1.234(6)		

Symmetry codes: 1 = 1 – X, 1 – Y,1 – Z; 2 = –X, –Y,1 – Z; 3 = –1/2+X,1/2 – Y, –1/2+Z; 4 = +X,1+Y,+Z; 5 = 1 – X,1 – Y,1 – Z; 6 = 1/2+X,1/2 – Y,1/2+Z; 7 = +X, –1+Y,+Z

Table S2. Selected bond lengths for compound **1**.

Bond	Angles (°)	Bond	Angles (°)
S(1)#1-Ag(1)-S(1)#3	100.85(5)	O(5)-N(2)-O(3)	118.8(5)
S(1)#2-Ag(1)-S(1)#3	141.85(5)	O(4)-N(2)-O(5)	120.9(5)
S(1)#1-Ag(1)-S(1)#2	100.29(4)	O(4)-N(2)-O(3)	120.3(5)
S(1)-Ag(2)-O(5)#4	133.12(10)	O(2)-N(1)-C(4)	117.8(6)
S(1)-Ag(2)-O(3)	95.89(11)	O(1)-N(1)-O(2)	123.8(5)
S(1)-Ag(2)-O(3)#4	115.02(11)	O(1)-N(1)-C(4)	118.4(5)
S(1)-Ag(2)-O(2)#5	98.19(11)	C(1)-S(1)-Ag(1)#2	111.18(16)
O(3)#4-Ag(2)-O(5)#4	50.04(12)	C(1)-S(1)-Ag(1)#3	104.95(16)
O(3)-Ag(2)-O(5)#4	109.14(13)	C(1)-S(1)-Ag(1)#6	105.73(15)
O(3)#4-Ag(2)-O(3)	149.08(19)	C(1)-S(1)-Ag(2)	105.00(15)
O(5)#4-Ag(2)-O(2)#5	115.74(14)	C(2)-C(1)-S(1)	120.7(4)
O(3)-Ag(2)-O(2)#5	98.40(16)	C(2)-C(1)-C(6)	118.9(4)
O(3)#4-Ag(2)-O(2)#5	77.21(15)	C(6)-C(1)-S(1)	120.4(4)
O(5)-Ag(1)-S(1)#1	97.31(10)	C(1)-C(2)-H(2)	119.6
O(5)-Ag(1)-S(1)#2	113.18(9)	C(3)-C(2)-C(1)	120.8(5)
O(5)-Ag(1)-S(1)#3	95.13(9)	C(3)-C(2)-H(2)	119.6
Ag(1)#3-S(1)-Ag(1)#6	79.62(4)	C(3)-C(4)-N(1)	119.2(5)
Ag(1)#3-S(1)-Ag(1)#2	141.85(5)	C(3)-C(4)-C(5)	122.3(5)
Ag(1)#2-S(1)-Ag(1)#6	79.24(4)	C(5)-C(4)-N(1)	118.5(5)
Ag(1)-O(5)-Ag(2)#7	158.15(17)	C(2)-C(3)-H(3)	120.6
Ag(2)-S(1)-Ag(1)#2	82.20(4)	C(4)-C(3)-C(2)	118.7(5)
Ag(2)-S(1)-Ag(1)#6	148.18(5)	C(4)-C(3)-H(3)	120.6
Ag(2)-S(1)-Ag(1)#3	100.22(5)	C(1)-C(6)-H(6)	119.9
Ag(2)#7-O(3)-Ag(2)	149.08(19)	C(5)-C(6)-C(1)	120.2(5)
N(2)-O(5)-Ag(1)	106.5(3)	C(5)-C(6)-H(6)	119.9
N(2)-O(5)-Ag(2)#7	95.2(3)	C(4)-C(5)-C(6)	119.1(5)
N(2)-O(3)-Ag(2)	101.5(3)	C(4)-C(5)-H(5)	120.4
N(2)-O(3)-Ag(2)#7	95.9(3)	C(6)-C(5)-H(5)	120.4

Symmetry codes: 1 = –1/2 + X, 1/2– Y,–1/2+Z; 2 = – X,1– Y,1– Z; 3 = – X,– Y,1– Z; 4 = +X,1+Y,+Z; 5 = 1– X,1– Y,1– Z; 6 = 1/2+X,1/2– Y,1/2+Z; 7 = +X,– 1+Y,+Z

Table S3. Recent progresses on high-performance humidity sensors.

Material	The highest response	Detected RH range	Res (s)/Rec (s)	Device type	Ref.
Single SnO_2	32	5.0%–85%	120–170 / 20–60	Resistive	[1]
$(NBu_4)_2Cu_2(dhbq)_3$	2.1×10^4	30%–90%	54 / 6	Resistive	[2]
Graphene (CVD)	0.003	1%–96%	0.6 / 0.4	Resistive	[3]
Multilayer graphene	0.17	15%–80%	< 1	Resistive	[4]
GO	33.2	0%–95%	50 / 79	Resistive	[5]
rGO	0.353	20%–95%		Resistive	[6]
rGO/MoS_2	24.94	5%–85%	6.3 / 30.8	Resistive	[7]
Black phosphorus/graphene	0.434	15%–70%	9 / 30	Resistive	[8]
Borophene–graphene	42	0%–85%	10.5 / 8.3	Resistive	[9]
Few-layered graphene	0.06	0%–85%		Resistive	[9]
α´-4H borophene	1.5	67%–85%	2.3 / 0.7	Resistive	[9]
graphene/Ag colloids	0.035	12%-97%	54 / 132	Resistive	[10]
WS_2	2357	20%–90%	5 / 6	Resistive	[11]
TaS_2 nanosheets	187.6	11%–95%	0.6 / 2.0	Resistive	[12]
cellulose	10^4	20%–90%	1500 /–	Resistive	[13]
cellulose	1647	41.5%–91.5%	19 / 472	Resistive	[14]
SiO_2 NPs	10^4	10%–93%	31.4 / 6.5	Resistive	[15]

GNCP	2×10^4	0%–97%	20 ms/17 ms	Resistive	[16]
Carbon nanocoils	0.12	4%–95%	1.9 / 1.5	Resistive	[17]
MWCNTs/PLL	6.6	0%–91.5%	30 / 2	Resistive	[18]
$SnWO_4$-SnO_2	10^3	5%–98%	30 / 100	Capacitive	[19]
Graphene/TiO_2	10^3	12%–90%	128 / 68	Capacitive	[20]
Li/SBA-15	$10^{3.5}$	11%–95%	60 / 180	Capacitive	[21]
CdS/ZnO	10^3	11%–95%	110 / 32	Capacitive	[22]
Nanometer zirconia thick film	10^4	11%–98%	130 / 60	Capacitive	[23]
TiO_2 porous ceramic	10^4	11%–95%	32 / 131	Capacitive	[24]
LiCl-C_3N_4	10^3	11%–95%	0.9 / 1.4	Capacitive	[25]
Au/g-C_3N_4	10^5	11%–95%	46.4 / 42.8	Capacitive	[26]
LiCl/Pebax	10^4	11%–95%	30 / 80	Capacitive	[27]
NiAl-LDH/PANI/SDS	10^4	11%–95%	4 / 25	Capacitive	[28]
TiO_2 NPs/PPy	10^2	30%–90%	40 / 20	Capacitive	[29]
SiO_2/poly(AMPS)	10^4	30%–90%	60 / 120	Capacitive	[30]
QC-P4VP/PANI	10^3	1%–98%	24 / 35	Capacitive	[31]
LiCl/PETMP-DVB	3×10^2	11%–95%	3.5 / 63	Capacitive	[32]
SnS_2	1.13×10^4	11%–95%	85 / 6	Resistive	[33]
SnSe nanosheet	1.4×10^4	11%–95%	22 / 7	Resistive	[34]
LiCl:SnSe nanosheet	3.12×10^3	11%–95%	12 / 4	Resistive	[34]
NaCl-KIT-6	10^5	11%–95%		Capacitive	[35]
KCl-doped SnO_2-NF	10^5	11%–95%	5 / 6	Capacitive	[36]

LiCl@UiO-66-NH_2	10^4	33%–95%	6 / 18	Capacitive	[37]
Ag(SPh-NO_2)•$AgNO_3$	**10^6**	**10%-90%**	**198/5**	**Resisitive**	**This work**

Table S4. Equivalent circuits and the dominating conductive ions under various RH.

RH	Equivalent Circuits	Dominating Conducive Species
40%	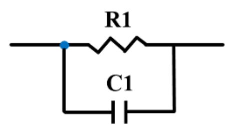	H^+
60%, 75%	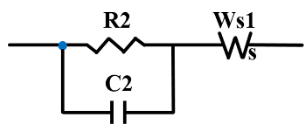	H_3O^+
85%, 90%, 95%	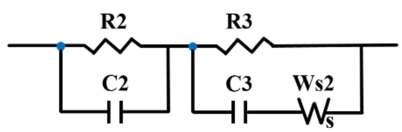	H_3O^+& Ag^+

Detailed method of humidity control.

The sensor characterization was conducted by a home-made system as shown in Figure. S1. The control of the relative humidity was based on the dynamic volumetric method. It takes ~0.65 min to fulfil the quartz chamber when the gas flow was 600 mL/min. MFC1, MFC2 and MFC3 in Figure. S1 were utilized to control the Carrier Gas (dry air for blank measurement), Mixed Gas (dry air for mixing with humidity gas) and Bubbling Gas (dry air for bubbling into the water). The target moisture gas with specific relative humidity (RH %) was produced by mixing the Bubbling Gas and Mixed Gas in a proper ratio controlled by the mass flow controllers (CS-

200C, Beijing Sevenstar Qualiflow Electronic Equipment Manufacturing Co., Ltd., China). The relative humidity was calculated by following equation：

$$X\%\ (RH) = \frac{Bubbling\ gas\ flow}{Mixed\ gas\ flow + Bubbling\ gas\ flow} \cdot 100\%$$

After the equilibration time of 7 min, the target relative humidity gas was introduced into the quartz tube with the chemiresistive sensor inside. The constant flow was 600 mL/min, the bias on the sensor was 1 V and the current was recorded using Keithley 2602B Source meter.

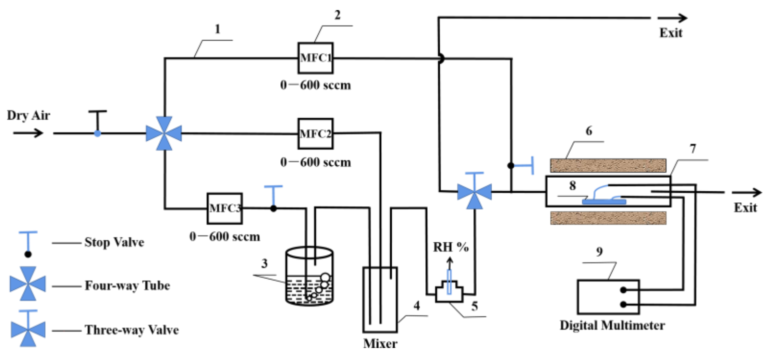

Figure S1. Schematic diagram of the home-made set-up used to measure the humidity sensor performance.(1-Stainless Steel Tube; 2-Mass Flow Controller; 3-Water Bubbling Bottle; 4-Gas Mixer; 5-Relative Humidity Monitor; 6-Tube Furnace; 7-Quartz Tube; 8-Gas Sensor for testing; 9-Digital Multimeter, Keithley 4200 source meter).

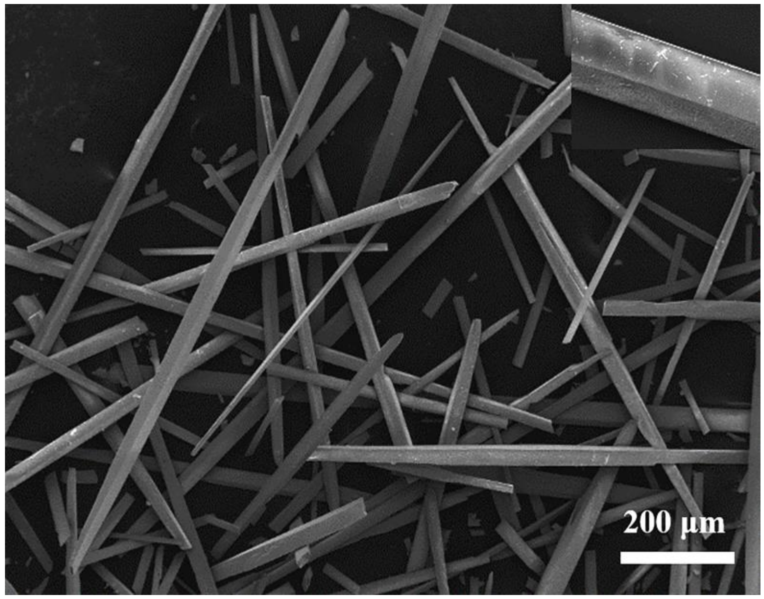

Figure S2. SEM image of compound **1** crystals.

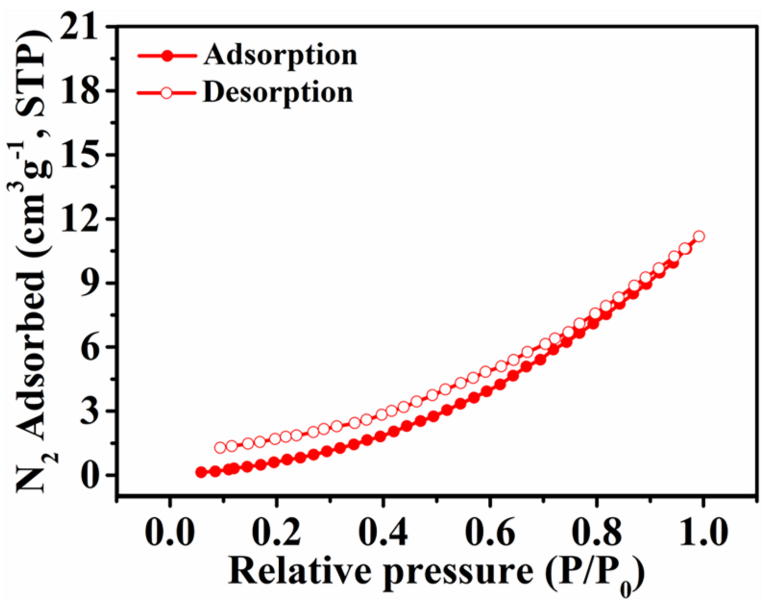

Figure S3. N_2 adsorption–desorption measurement at 77 K of compound **1**.

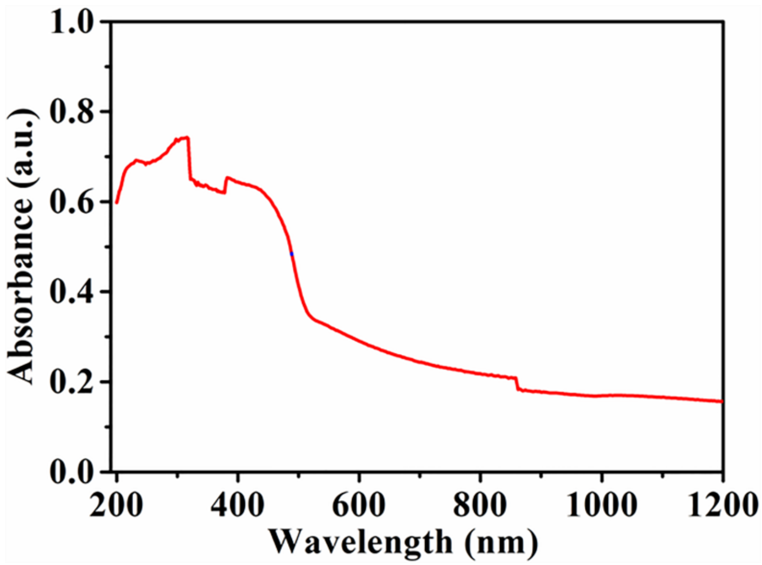

Figure S4. UV-Vis DRS of compound **1**.

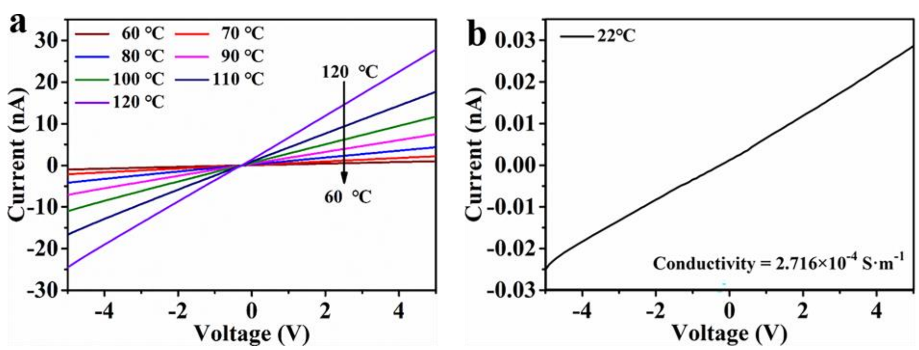

Figure S5. (a) Temperature-dependent I-V curves and (b) room temperature electronic conductivity of single crystal **1**.

Possible conduction path for electron in the structure of crystal 1

Refer to the research of Lu et al,[39] they reported a new highly conductive MOF, $[Cu_2$(6-Hmna)(6-mn)•$NH_4]_n$, composed of a 2D (-Cu-S-)n plane. Through electronic structure calculation, they determined that the high conductivity of this material comes from a highly dense pathway generated from (-Cu-S-)n For the structure of Ag(SPh-NO_2)•$AgNO_3$, the (-Ag-S-

)n plane contained in its inorganic layer is similar to the (-Cu-S-)n plane. Therefore, as shown in Figure S6, we speculate that the possible conduction path of electrons is the (-Ag-S-)n chain.

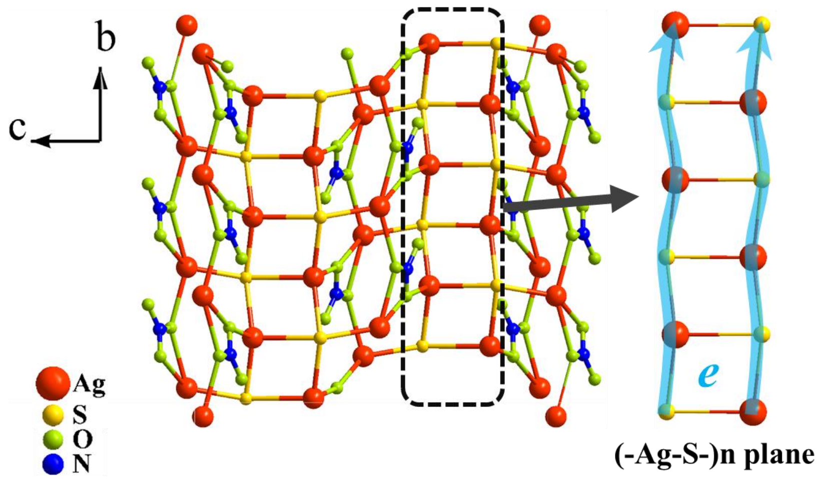

Figure S6. The possible conduction path for electron in the structure of Ag(SPh-NO_2)•$AgNO_3$.

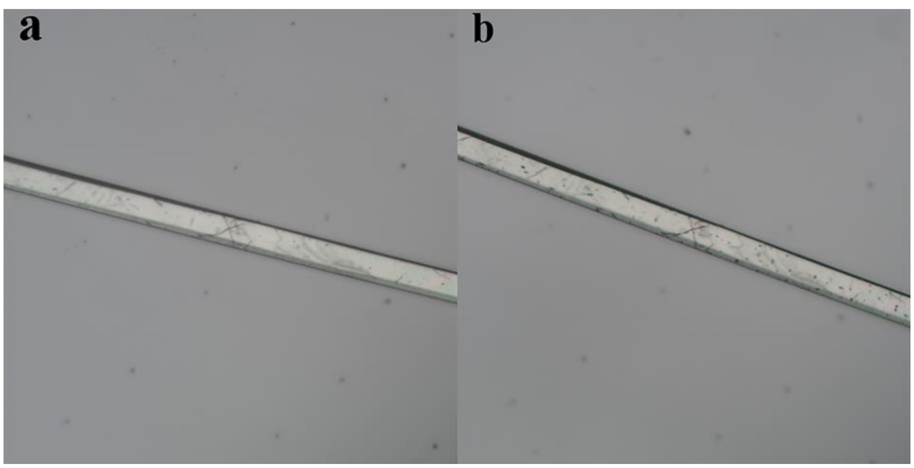

Figure S7. Optical photos of compound **1** crystal (a) before and (b) after under 100% RH 1 days.

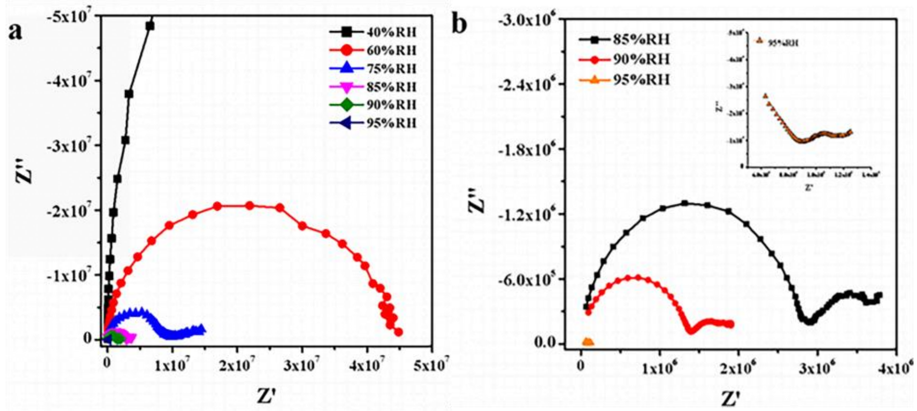

Figure S8. Nyquist plots for compound **1**obtained from 0.1Hz to 10^5 Hz at various RH.

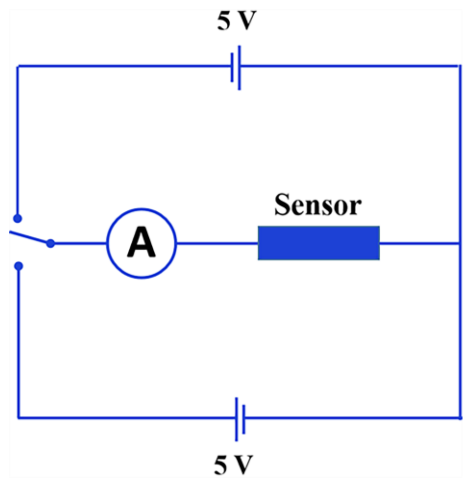

Figure S9. The DC circuit of the reverse polarity method.

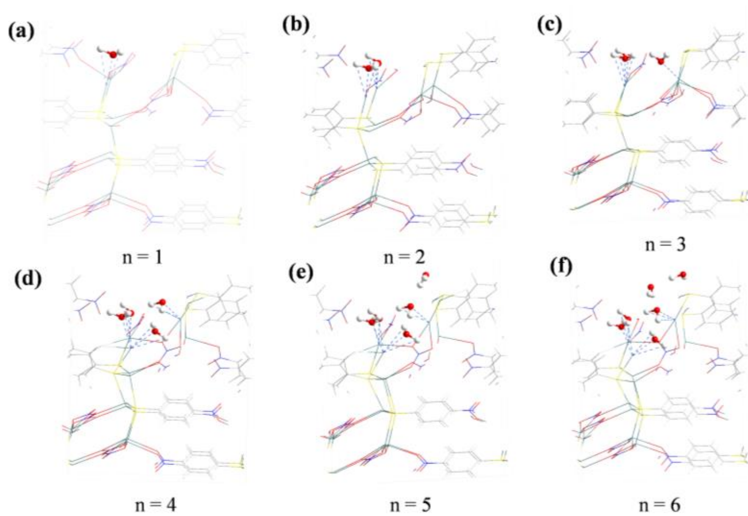

Figure S10. The structure models simulated for gibbs free energy (Δ G) calculation of reaction

$Ag(SPh\text{-}NO_2)\bullet AgNO_3 + nH_2O \rightarrow AgNO_3 + Ag(SPh\text{-}NO_2)\bullet nH_2O$ (n = 1, 2, 3, 4, 5, 6)

REFERENCES

(1) Kuang, Q.; Lao, C.; Wang, Z.-L.; Xie, Z.; Zheng, L.; High-Sensitivity Humidity Sensor Based on a Single SnO_2 Nanowire. *J. Am. Chem. Soc.***2007**, *129*, 6070–6071.

(2) Lv, X.-J.; Yao, M.-S.; Wang, G.-E.; Li, Y.-Z.; Xu, G. A new 3D cupric coordination polymer as chemiresistor humidity sensor: narrow hysteresis, high sensitivity, fast response and recovery. *Sci. China. Chem.***2017**, *60*, 1197-1204.

(3) Smith, A. D.; Elgammal, K.; Niklaus, F.; Delin, A.; Fischer, A. C.; Vaziri, S.; Forsberg, F.; Rasander, M.; Hugosson, H.; Bergqvist, L.; Schroder, S.; Kataria, S.; Ostling, M.; Lemme, M. C. Resistive graphene humidity sensors with rapid and direct electrical readout. *Nanoscale.***2015**, *7*, 19099-19109.

(4) Popov, V. I.; Nikolaev, D. V.; Timofeev, V. B.; Smagulova, S. A.; Antonova, I. V. Graphene-based humidity sensors: the origin of alternating resistance change. *Nanotechnology.***2017**, *28*, 355501.

(5) Feng, X.; Chen, W.; Yan, L. Free-standing dried foam films of graphene oxide for humidity sensing. *Sensors and Actuators B: Chemical.***2015**, *215*, 316-322.

(6) Phan, D. T.; Chung, G. S. Effects of rapid thermal annealing on humidity sensor based on graphene oxide thin films. *Sensors and Actuators B: Chemical.***2015**, *220*, 1050-1055.

(7) Park, S. Y.; Kim, Y. H.; Lee, S. Y.; Sohn, W.; Lee, J. E.; Kim, D. H.; Shim, Y. S.; Kwon, K. C.; Choi, K. S.; Yoo, H. J.; Suh, J. M.; Ko, M.; Lee, J. H.; Lee, M. J.; Kim, S. Y.; Lee, M. H.; Jang, H. W. Highly selective and sensitive chemoresistive humidity sensors based on rGO/MoS_2 van der Waals composites. *J. Mater. Chem. A.***2018**, *6*, 5016-5024.

(8) Phan, D. T.; Park, I.; Park, A. R.; Park, C. M.; Jeon, K. J. Black P/graphene hybrid: A fast response humidity sensor with good reversibility and stability. *Sci. Rep.***2017**, *7*, 10561.

(9) Hou, C.; Tai, G.-A.; Liu, B.; Wu, Z.; Yin, Y. Borophene-grapheneheterostructure: Preparation and ultrasensitive humidity sensing. *Nano Res.***2020**.

(10) Pang, Y.; Jian, J.; Tu, T.; Yang, Z.; Ling, J.; Li, Y.; Wang, X.; Qiao, Y.; Tian, H.; Yang, Y.; Ren, T. L. Wearable humidity sensor based on porous graphene network for respiration monitoring. *Biosens and Bioelectron.***2018**, *116*, 123-129.

(11) Guo, H.; Lan, C.; Zhou, Z.; Sun, P.; Wei, D.; Li, C. Transparent, flexible, and stretchable WS_2 based humidity sensors for electronic skin. *Nanoscale.***2017**, *9*, 6246-6253.

(12) Feng, Y.; Gong, S.; Du, E.; Yu, K.; Ren, J.; Wang, Z.; Zhu, Z. TaS_2nanosheet-based ultrafast response and flexible humidity sensor for multifunctional applications. *J. Mater. Chem. C.***2019**, *7*, 9284-9292.

(13) Guder, F.; Ainla, A.; Redston, J.; Mosadegh, B.; Glavan, A.; Martin, T. J.; Whitesides, G. M. Paper-Based Electrical Respiration Sensor. *Angew. Chem. Int. Ed.***2016**, *55*, 5727-5732.

(14) Duan, Z.; Jiang, Y.; Yan, M.; Wang, S.; Yuan, Z.; Zhao, Q.; Sun, P.; Xie, G.; Du, X.; Tai, H. Facile, Flexible, Cost-Saving, and Environment-Friendly Paper-Based Humidity Sensor for Multifunctional Applications. *ACS Appl. Mater. Interfaces.***2019**, *11*, 21840-21849.

(15) Kano, S.; Fujii, M. All-Painting Process to Produce Respiration Sensor Using Humidity-Sensitive Nanoparticle Film and Graphite Trace. *ACS Sustainable Chem. Eng.***2018**, *6*, 12217-12223.

(16) He, J.; Xiao, P.; Shi, J.; Liang, Y.; Lu, W.; Chen, Y.; Wang, W.; Théato, P.; Kuo, S.-W.; Chen, T. High Performance Humidity Fluctuation Sensor for Wearable Devices via a Bioinspired Atomic-Precise Tunable Graphene-Polymer Heterogeneous Sensing Junction. *Chem. Mater.***2018**, *30*, 4343-4354.

(17) Wu, J.; Sun, Y. M.; Wu, Z.; Li, X.; Wang, N.; Tao, K.; Wang, G. P. Carbon Nanocoil-Based Fast-Response and Flexible Humidity Sensor for Multifunctional Applications. *ACS Appl. Mater. Interfaces.***2019**, *11*, 4242-4251.

(18) Zhao, Q.; Yuan, Z.; Duan, Z.; Jiang, Y.; Li, X.; Li, Z.; Tai, H. An ingenious strategy for improving humidity sensing properties of multi-walled carbon nanotubes via poly-L-lysine modification. *Sensors and Actuators B: Chemical.* **2019**, *289*, 182-185.

(19) Sundaram, R. Comparative study on micromorphology and humidity sensitive properties of thick film and disc humidity sensors based on semiconducting $SnWO_4$–SnO_2 composites. *Sensors and Actuators B: Chemical.* **2007**, *124*, 429-436.

(20) Lin, W.-D.; Liao, C.-T.; Chang, T.-C.; Chen, S.-H.; Wu, R.-J. Humidity sensing properties of novel graphene/TiO_2 composites by sol–gel process. *Sensors and Actuators B: Chemical.* **2015**, *209*, 555-561.

(21) Zhang, T.; Wang, R.; Geng, W.; Li, X.; Qi, Q.; He, Y.; Wang, S. Study on humidity sensing properties based on composite materials of Li-doped mesoporous silica A-SBA-15. *Sensors and Actuators B: Chemical.* **2008**, *128*, 482-487.

(22) Feng, M.-H.; Wang, W.-C.; Li, X.-J. Capacitive humidity sensing properties of CdS/ZnO sesame-seed-candy structure grown on silicon nanoporous pillar array. *Journal of Alloys and Compounds.* **2017**, *698*, 94-98.

(23) Wang, J.; Su, M.-Y.; Qi, J.-Q.; Chang, L.-Q. Sensitivity and complex impedance of nanometer zirconia thick film humidity sensors. *Sensors and Actuators B: Chemical.* **2009**, *139*, 418-424.

(24) Wang, X.; Li, J.-H.; Li, Y.-L; Liu, L.-J.; Guan, W.-M. Emulsion-templated fully three-dimensional interconnected porous titania ceramics with excellent humidity sensing properties. *Sensors and Actuators B: Chemical.* **2016**, *237*, 894-898.

(25) Zhang, Z.; Huang, J.; Yuan, Q.; Dong, B. Intercalated graphitic carbon nitride: a fascinating two-dimensional nanomaterial for an ultra-sensitive humidity nanosensor. *Nanoscale.* **2014**, *6*, 9250-9256.

(26) Yu, S.; Zhang, H.; Chen, C.; Zhang, J.; Li, P. Preparation and mechanism investigation of highly sensitive humidity sensor based on two-dimensional porous Gold/Graphite carbon nitride nanoflake. *Sensors and Actuators B: Chemical.* **2020**, *307*, 127679.

(27) Liang, S.; He, X.; Wang, F.; Geng, W.; Fu, X.; Ren, J.; Jiang, X. Highly sensitive humidity sensors based on LiCl–Pebax 2533 composite nanofibers via electrospinning. *Sensors and Actuators B: Chemical.***2015**, *208*, 363-368.

(28) Li, X.-Z.; Liu, S.-R.; Guo, Y. Polyaniline-intercalated layered double hydroxides: synthesis and properties for humidity sensing. *RSC Adv.***2016**, *6*, 63099-63106.

(29) Su, P.-G.; Huang, L.-N. Humidity sensors based on TiO_2 nanoparticles/polypyrrole composite thin films. *Sensors and Actuators B: Chemical.***2007**, *123*, 501-507.

(30) Su, P.; Tsai, W. Humidity sensing and electrical properties of a composite material of nano-sized SiO_2 and poly(2-acrylamido-2-methylpropane sulfonate). *Sensors and Actuators B: Chemical.***2004**, *100*, 417-422.

(31) Li, Y.; Fan, K.; Ban, H.; Yang, M. Bilayer-structured composite sensor based on polyaniline and polyelectrolyte for sensitive detection of low humidity. *Synthetic Metals.***2015**, *199*, 51-57.

(32) Dai, J.; Zhang, T.; Qi, R.; Zhao, H.; Fei, T.; Lu, G. LiCl loaded cross-linked polymer composites by click reaction for humidity sensing. *Sensors and Actuators B: Chemical.***2017**, *253*, 361-367.

(33) Zhang, D.; Wang, M.; Zhang, W.; Li, Q. Flexible humidity sensing and portable applications based on $MoSe_2$nanoflowers/copper tungstate nanoparticles. S*ensors and Actuators B: Chemical.***2020**, *304*,127234.

(34) Zhu, K.; Tang, Y.; Zhong, X.; Xiong, L.; Zhang, Y.; Tan, C.; Song, H.; Wang, J. Improved Response/Recovery Time and Sensitivity of SnSeNanosheet Humidity Sensor by LiCl Incorporation. *Adv. Electron. Mater.***2020**, *6*, 1901330.

(35) He, X.; Geng, W.; Zhang, B.; Jia, L.; Duan, L.; Zhang, Q. Ultrahigh humidity sensitivity of NaCl-added 3D mesoporous silica KIT-6 and its sensing mechanism. *RSC Adv.* **2016**, *6*, 38391-38398.

(36) Song, X.; Qi, Q.; Zhang, T.; Wang, C. A humidity sensor based on KCl-doped SnO_2nanofibers. *Sensors and Actuators B: Chemical.* **2009**, *138*, 368-373.

(37) Zhang, Y.; Xiong, J.; Chen, C.; Li, Q.; Liu, J.; Zhang, Z. Regulating the dissociation of LiCl and transportation of Li ions within UiO-66-NH_2 framework for humidity sensing applications with superb comprehensive performances. *Journal of Alloys and Compounds.* **2020**, *818*, 152854.

(38) Sun, L.; Campbell, M. G.; Dincă, M. Electrically Conductive Porous Metal–Organic Frameworks. *Angewandte Chemie*. **2016**, *55*, 3566-3579.

(39) Pathak, A.; Shen, J. W.; Usman, M.; Wei, L. F.; Mendiratta, S.; Chang, Y. S.; Sainbileg, B.; Ngue, C. M.; Chen, R. S.; Hayashi, M.; Luo, T. T.; Chen, F. R.; Chen, K. H.; Tseng, T. W.; Chen, L. C.; Lu, K. L. Integration of a (-Cu-S-)n plane in a metal-organic framework affords high electrical conductivity. *Nat. Commun.* **2019**, *10*, 1721.